

## Catalyst Screening and Optimization Condition of Green Solvent for BHD Production using Ni-based Catalysts

Patravee Ounsuk, Sirapat Triampitak, Jitsinee Leetrakul, Kandis Sudsakorn and Anusorn Seubsai  
National Center of Excellence for Petroleum, Petrochemicals and Advance Material, Department of Chemical Engineering, Faculty of Engineering, Kasetsart University, Bangkok, Thailand

Chaiwat Prapainainar  
Department of Chemical Engineering, Faculty of Engineering, King Mongkut's University of Technology North Bangkok, Bangkok, Thailand  
Research and Development Center for Chemical Unit Operation and Catalyst Design, Science and Technology Research Institute, King Mongkut's University of Technology North Bangkok, Bangkok, Thailand

Paweena Prapainainar\*  
National Center of Excellence for Petroleum, Petrochemicals and Advance Material, Department of Chemical Engineering, Faculty of Engineering, Kasetsart University, Bangkok, Thailand  
Research Network of NANOTEC - KU on NanoCatalysts and NanoMaterials for Sustainable Energy and Environment, Kasetsart University, Bangkok, Thailand

\* Corresponding author. E-mail: fengpwn@ku.ac.th DOI: 10.14416/j.asep.2024.03.002  
Received: 30 October 2023; Revised: 10 December 2023; Accepted: 18 January 2024; Published online: 18 March 2024  
© 2024 King Mongkut's University of Technology North Bangkok. All Rights Reserved.

### Abstract

The high production costs associated with bio-hydrogenated diesel (BHD) have posed a major challenge. Considering this, the present research focused on the production of green solvents at lower pressures as a potential solution. Specifically, the synthesis of various catalysts, namely Ni/ $\gamma$ -Al<sub>2</sub>O<sub>3</sub>, Ni/C, NiMo/ $\gamma$ -Al<sub>2</sub>O<sub>3</sub>, NiMo/SiO<sub>2</sub>TiO<sub>2</sub>, and NiMo/C, was conducted to facilitate the hydrodeoxygenation reaction of methyl laurate into cyclohexane, leading to conversion into dodecane. The resulting green solvent was analyzed using GC-FID and GC-TCD techniques. Among the five catalysts tested, NiMo/C demonstrated superior performance, achieving a conversion rate of 64.61%, selectivity of 62.46%, and yield of 44.98%. The gas analysis conducted using GC-TCD revealed the production of carbon monoxide, methane, and carbon dioxide, aligning with the dodecane pathway theory. Further analysis of the NiMo/C catalyst was conducted using SEM, BET, and XRD techniques, while the Design of Expert program was used to identify more favorable conditions for dodecane production. Through this optimization process, significant improvements were achieved, resulting in a conversion rate of 98.26%, selectivity of 66.82%, and yield of 65.66% at 320 °C and 28 bar, with a reaction time of 6 h.

**Keywords:** Dodecane, Green solvent, Hydrodeoxygenation, Methyl laurate

### 1 Introduction

In the last decade, demand for petroleum-derived products has grown sharply [1]. However, concomitantly, there have been increasing concerns about energy supply and harmful environmental effects, such as

climate change and air pollution [2], [3]. Bio-base products obtained from renewable sources have drawn considerable attention to developing clean and alternative sources [4]. Dodecane is a hydrocarbon compound mainly produced from petroleum. It has various applications among which are as a fuel additive

and solvent and in the synthesis of specialty chemicals. However, it has a high cost and is a non-sustainable chemical [5]. The alternative to production of dodecane is deoxygenation of biomass feedstock, such as methyl laurate [6] and lauric acid [7], to produce paraffinic hydrocarbons through the reaction pathway of hydrodeoxygenation (HDO), decarbonylation (DCO), and decarboxylation (DCO<sub>2</sub>) [8] known as green solvent as shown in Equations (1)–(3).



Green solvents play a vital role in renewable diesel or biodiesel usage by providing environmentally friendly alternatives to conventional solvents. Nowadays, deoxygenation catalysts mainly include noble metals (such as palladium and platinum) [8]–[10] and non-noble metals (such as nickel and molybdenum) [11]–[13]. These catalysts can adsorb oxygenated compounds, facilitate the cleavage of carbon-oxygen bonds, and promote hydrogenation reactions, ultimately leading to the production of deoxygenated hydrocarbons [14]. Noble metals have demonstrated excellent catalytic activity in deoxygenation reactions [15]. For example, a Pd/C catalyst produced the highest catalytic performance on lauric acid deoxygenation with above 95% of selectivity of the desired products [7]. Similarly, for a Pt-metal catalyst, Kon *et al.* [16] studied the deoxygenation of lauric acid to n-dodecane which had a high yield of 99%. Nevertheless, due to certain disadvantages, such as the high cost, especially in large-scale industrial applications, non-noble metal catalysts are favored due to their considerably lower cost compared to noble metal catalysts, without requiring major compromises in the levels of the desired outcomes. For example, a 10 wt.% Ni/ $\gamma$ -Al<sub>2</sub>O<sub>3</sub> catalyst produced good HDO performance, with a methyl laurate conversion rate of 91.1% at a reaction temperature of 400 °C and pressure of 20 bar, with the main products being decane, undecane, dodecane, dodecanol, and dodecanoic acid [17]. The deoxygenation of methyl laurate using a Ni/TiO<sub>2</sub> catalyst reported activity with a conversion of 50% [18]. A bi-metal catalyst was used to improve

the performance of this reaction, with the Ni-Mo/SiO<sub>2</sub> catalyst producing methyl laurate conversion of 75% and selectivity of dodecane and undecane of 75% [19]. Furthermore, a Ni-Mo/SiO<sub>2</sub>-TiO<sub>2</sub> catalyst produced methyl laurate conversion of 100% and a dodecane yield of 96.3% [18].

Several relevant variables can substantially influence the outcome of a deoxygenation reaction. Optimizing these variables is essential to achieve the desired product formation with both high yield and selectivity in deoxygenation reactions. RSM is a statistical method that uses the minimum of quantitative data and can assist in overcoming the constraints of any relationships between multivariate parameters and their responses. Thus, RSM has been used to investigate the effects of the deoxygenation reaction, such as temperature, pressure, solvent, and reaction time [20]–[22]. CCD [23] and BBD [24] are widely used experimental approaches. BBD requires fewer experiments than CCD; however, CCD has a star point ( $\pm \alpha$ ) that can help to estimate the nonlinearity of responses [25]. Optimization is integral to achieving cost-effective production, through minimizing expenses while maximizing the yield.

This study investigated the effects of mono-metal and bi-metal catalysts supported on gamma alumina, carbon, and silicon dioxide-titanium dioxide on the deoxygenation of methyl laurate to select the most efficacious catalyst. Then, the optimum conditions of the selected catalyst were determined using the Design of Expert program and central composite design (CCD) techniques with the 2 factors of temperature and pressure. A schematic diagram of the investigation pathway is shown in Figure 1.

## 2 Experiment

### 2.1 Material

The precursors used to synthesize the support were tetrabutyl orthotitanate (C<sub>16</sub>H<sub>3</sub>6O<sub>4</sub>Ti, TCI) and tetraethyl orthosilicate (SiC<sub>8</sub>H<sub>2</sub>0O<sub>4</sub>), both purchased from Sigma Aldrich. The catalyst precursors were nickel nitrate hexahydrate (Ni(NO<sub>3</sub>)<sub>2</sub>·6H<sub>2</sub>O, LOBA Chemie Pvt. Ltd.) and ammonium molybdate tetrahydrate ((NH<sub>4</sub>)<sub>6</sub>Mo<sub>7</sub>O<sub>24</sub>·4H<sub>2</sub>O, KemAus). Other materials used were methyl laurate, aluminum oxide, activated carbon and ammonium hydroxide purchased from TCI,

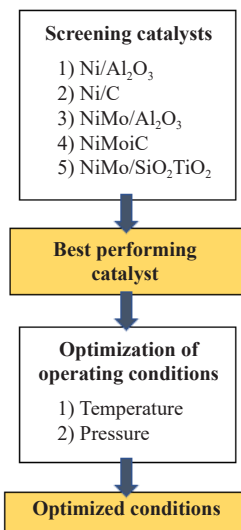


**Figure 1:** Schematic diagram of investigation pathway.

KemAus, Cabot, and PanReac AppliChem, respectively. Cyclohexane and acetone were provided by ACI Labscan. Eicosane and alkane standard solution C<sub>8</sub>–C<sub>20</sub> were purchased from Sigma Aldrich.

## 2.2 Catalyst synthesis

### 2.2.1 SiO<sub>2</sub>-TiO<sub>2</sub> support

Tetrabutyl titanate and tetraethyl orthosilicate were dissolved in distilled water (weight ratio 1:1) and stirred at 40 °C. Then 37 wt.% NH<sub>3</sub>·H<sub>2</sub>O was slowly dropped into the solution under continuous stirring until the pH value was within 9–10. The sample was washed, vacuum-filtered, and then dried at 100 °C for 12 h. Finally, the other species, such as tetrabutyl, tetraethyl, and oxygen atoms, were eliminated from the sample by calcining at 400 °C for 4 h to obtain the SiO<sub>2</sub>-TiO<sub>2</sub> support.

### 2.2.2 Preparation of catalysts

The monometallic catalysts were prepared using an aqueous solution of 10 wt % Ni impregnated over aluminum oxide (γ-Al<sub>2</sub>O<sub>3</sub>) and a carbon support to obtain Ni/Al<sub>2</sub>O<sub>3</sub> and Ni/C. These solutions were stirred for 30 min and dried at 110 °C overnight. Ni/Al<sub>2</sub>O<sub>3</sub> and Ni/C were calcined at 550 °C for 4 h and at 350 °C for 3 h, respectively.

The bimetallic catalysts were prepared using an aqueous mixture solution of 10 wt % Ni and 3 wt % Mo impregnated over support γ-Al<sub>2</sub>O<sub>3</sub>, C, and SiO<sub>2</sub>-TiO<sub>2</sub>. These solutions were stirred for 30 min and dried at 110 °C overnight. NiMo/Al<sub>2</sub>O<sub>3</sub>, NiMo/C, and NiMo/SiO<sub>2</sub>TiO<sub>2</sub> were calcined at 550 °C for 4 h, 500 °C for 1 h, and 450 °C for 6 h, respectively.

## 2.3 Catalyst screening

An amount (0.1 g) of each catalyst was reduced in a tube furnace with an H<sub>2</sub> flow rate of 30 mL/Al<sub>2</sub>O<sub>3</sub> catalysts were reduced at 350 °C for 3 h and 500 °C for 1 h, respectively. [17], [18], [26]

The reduced catalysts were combined with 0.5 g of methyl laurate and 30 mL of cyclohexane as a solvent and loaded into 50 mL Parr reactor 5500 series to perform deoxygenation of the methyl laurate in batch mode. The reactants were purged using N<sub>2</sub> for 20 min and compressed from atmospheric pressure using H<sub>2</sub> to a pressure of 25 bar. Subsequently, the Parr reactor was heated to 300 °C and held at this temperature for 6 h, during which time, the mixture in the reactor was stirred mechanically at 120 rpm. The product was collected after 6 h of reaction. The liquid phase product was separated using centrifugation and the gas phase product was kept in a sampling bag.

The liquid products were identified using gas chromatography (model GC-2014C; Shimadzu) and flame ionization detection (GC-FID) fitted with a DB-5HT column. Samples (each 1 μL) of diluted liquid products were injected into the instrument using eicosane as the internal standard and helium as the carrier gas. The initial temperature was 100 °C, then increased to 210 °C at a rate of 10 °C/min and held for 4 min after which it was again increased to 280 °C at a rate of 10 °C/min and held for 2 min.

The gas phase products were analyzed using gas chromatography (model GC-14A; Shimadzu) and thermal conductivity detection (GC-TCD) equipped with a Porapak U packed column. Conversion, selectivity and yield were calculated using Equations (4)–(6), respectively:

Conversion (%) =

$$\frac{n_{\text{methyl laurate, in}} - n_{\text{methyl laurate, out}}}{n_{\text{methyl laurate, in}}} \times 100 \quad (4)$$

$$\text{Selectivity (\%)} = \frac{n_{\text{desired product, out}}}{n_{\text{total product, out}}} \times 100 \quad (5)$$

$$\text{Yield (\%)} = \frac{\% \text{Conversion} \times \% \text{Selectivity}}{100} \quad (6)$$

Where  $n$  is the amount of compound (mol)

## 2.4 Catalyst characterization

Field emission scanning electron microscopy/energy dispersive (FE-SEM/EDS) images were obtained using an FEI- Quanta 450 apparatus (JEOL Ltd.) to detect the surface morphology. They were performed with a 20 keV electron beam connected with an Oxford X-Max EDX detector (JEOL Ltd.). X-ray diffraction (XRD) patterns were recorded on a Bruker AXS GmbH, D8 advance target diffractometer equipped with a Cu-K $\alpha$  radiation source ( $\lambda = 1.5406 \text{ \AA}$ ) over the  $2\theta$  range of  $10\text{--}80^\circ$  at a scanning speed of  $4^\circ/\text{min}$  and a step size of  $0.03^\circ$ . The specific surface area and pore distribution of the catalysts were determined using the Brunauer-Emmet-Teller (BET) method and a N $_2$  adsorption-desorption analyzer based on Micromeritics, 3 Flex surface characterization (Micromeritics, USA). The transmission electron microscopy (TEM) images were obtained using a JEOL, JEM-2010 apparatus at an acceleration voltage of 300 kV.

## 2.5 Design of experiment

A central composite design (CCD) was used to meticulously plan and investigate the impact of temperature and pressure as the two primary variables. The temperature was set within the range of  $280\text{--}320^\circ\text{C}$ , while the hydrogen pressure was selected within the range of  $22\text{--}28$  bar. The Design Expert version 13 program facilitated the formulation of the experimental conditions required for the synthesis of dodecane. The specific conditions determined by the program are presented in Table 1.

**Table 1:** Summary of variables used in CCD

Variables	Unit	Coded and Actual Values				
		- $\alpha$	-1	0	1	$\alpha$
Temperature	$^\circ\text{C}$	272	280	300	320	328
Pressure	Bar	21	22	25	28	29

Mathematical models were presented using linear, quadratic, and interactive components, as shown in Equations (7):

$$y = \beta_0 + \sum_{i=1}^k \beta_i x_i + \sum_{i=1}^k \beta_{ii} x_i^2 + \sum_{i=1}^k \sum_{j=1}^k \beta_{ij} x_i x_j + \varepsilon \quad (7)$$

where  $y$  is the dodecane yield (response factor);  $\beta_0$  is the coefficient denoting the intercept;  $\beta_i$ ,  $\beta_{ii}$ , and  $\beta_{ij}$ , are the regression coefficients of the model;  $x_i$ , and  $x_j$  are independent variables; and  $\varepsilon$  is the random error. [27]

## 3 Results and Discussion

### 3.1 Catalytic activity test

The methyl laurate deoxygenation over different types of catalyst was done under conditions of  $300^\circ\text{C}$ , 25 bar, and 6 h following the work from Fu *et al.* [18], with the current results presented in Table 2. These results varied from their results perhaps because of the different reactor size and stirring speed.

**Table 2:** Comparison of catalysts used for methyl laurate deoxygenation

Catalyst	Conversion (%)	Yield (%)	
		Undecane	Dodecane
Ni/Al $_2$ O $_3$	37.32	36.82	0.50
Ni/C	31.58	29.00	2.58
NiMo/Al $_2$ O $_3$	98.69	80.15	18.54
NiMo/C	98.57	53.59	44.98
NiMo/SiO $_2$ TiO $_2$	100.00	73.17	26.83

Complete conversion of methyl laurate was achieved for the NiMo/SiO $_2$ TiO $_2$  catalyst and decreased when using NiMo/Al $_2$ O $_3$ , NiMo/C, Ni/Al $_2$ O $_3$ , and Ni/C, respectively. This reaction resulted in dodecane as the main product, with the co-product being undecane. However, the highest yield of the desired product (dodecane) to use in green diesel production was achieved using NiMo/C, with a methyl laurate conversion of 98.57% and a dodecane yield of 44.98%. In addition, the bimetallic catalysts (NiMo/Al $_2$ O $_3$ , NiMo/C, and NiMo/SiO $_2$ TiO $_2$ ) had conversion and yield results for dodecane that were higher than from using the monometallic catalysts (Ni/Al $_2$ O $_3$  and Ni/C). This was a result of the synergistic effect between the Ni and Mo metals that improved

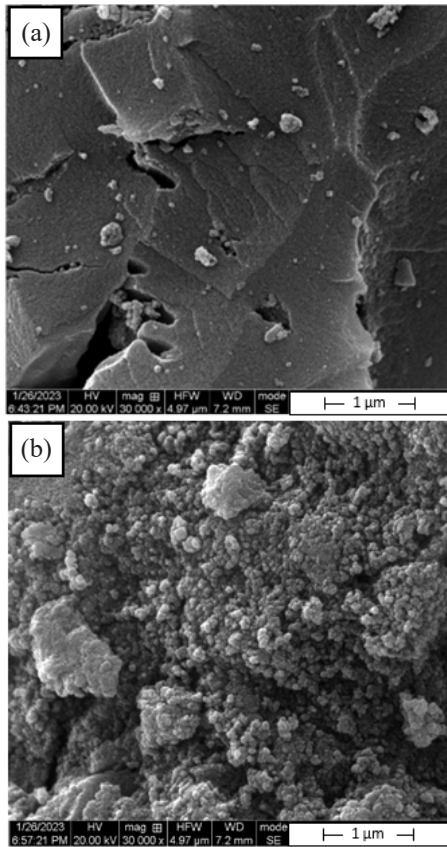


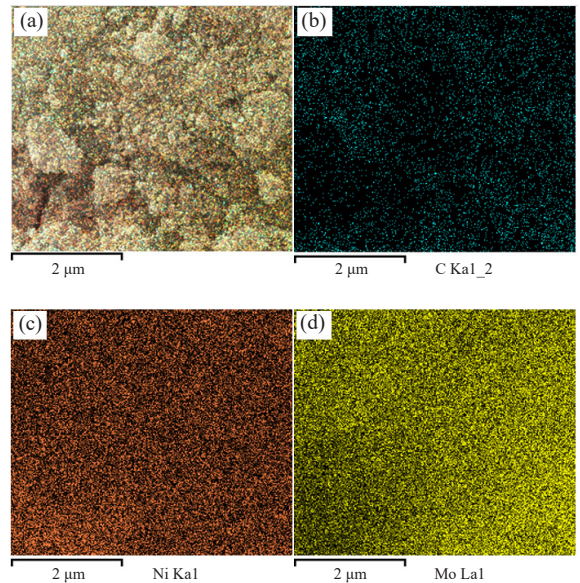
**Figure 2:** FE-SEM images of carbon support (a) and NiMo/C catalyst (b) at 30,000x.

hydrodeoxygenation [28].

The confirmation of the reaction pathway was established through the analysis of the distribution of gaseous products based on GC-TCD. Methane ( $\text{CH}_4$ ) and carbon dioxide ( $\text{CO}_2$ ) were found in the gaseous product, suggesting that possible reaction pathways were a decarbonylation reaction and a methanation reaction. The  $\text{CO}_2$  was released following the removal of the carboxyl group ( $-\text{COOH}$ ) of lauric acid and  $\text{CH}_4$  was produced from the reaction between  $\text{CO}$  or  $\text{CO}_2$  and fatty acids [29].

### 3.2 Characterization of NiMo/C catalyst

The result of the catalytic activity test showed that the NiMo/C catalyst had the highest performance based on the dodecane yield. Therefore, the NiMo/C catalyst was analyzed in detail.



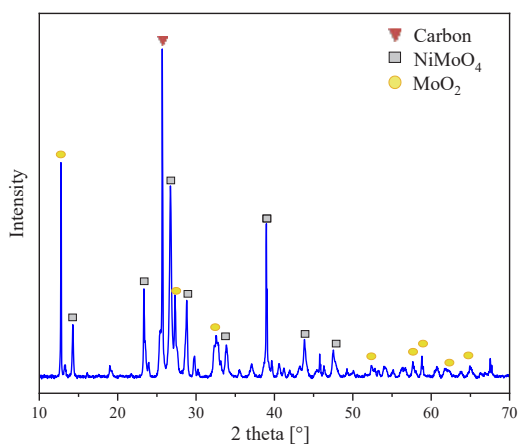
**Figure 3:** EDS mapping of NiMo/C catalyst. Layered image (a); C map (b); Ni map (c); Mo map (d).

Figure 2 shows the SEM images of the carbon support and NiMo/C catalyst. The carbon support [Figure 1(a)] had a smooth surface that was covered with pores. At greater magnification, the particles of Ni and Mo on the carbon support [Figure 1(b)] were spherical and stacked compactly on the surface.

Figure 3 presents the EDS analysis of the Ni, Mo, and C in the NiMo/C sample. Dot mapping revealed that Ni and Mo metals were highly dispersed on the carbon support. The elemental composition in the NiMo/C catalyst was 26.97 wt% Ni, 32.12 wt% Mo, and 40.91 wt% C.

The crystallinity and phase identification of the carbon support and NiMo/C catalyst were determined based on XRD patterns, as shown in Figure 4. The carbon support displayed diffraction peaks at 24.7 and 43.0, which were assigned to (002) and (101) of graphitic carbon [30]. After loading the Ni and Mo on the C support, the characteristic peaks corresponding to  $\text{NiMoO}_4$  (JCPDS file # 31-0902) and  $\text{MoO}_3$  (PFD#32-0671) were present as the main diffraction peaks at 12.77, 14.28, 23.35, 27.30, 28.81, 32.55, 43.84 and 47.24, suggesting that the metals had formed on the surface of the support. [31], [32]

The BET test using nitrogen adsorption revealed the textural properties of the synthesized nano-catalysts.



**Figure 4:** XRD pattern of NiMo/C catalyst.

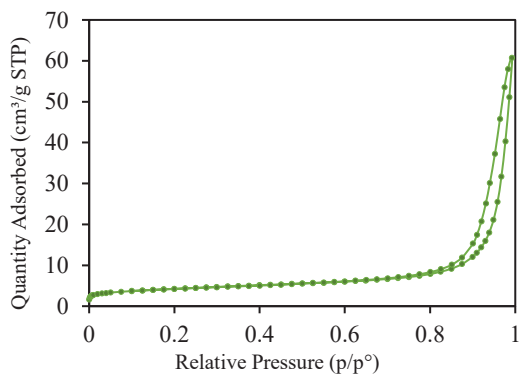


**Figure 5:** BET isotherm of NiMo/C catalyst.

The NiMo/C catalyst had a specific surface area of  $14.51 \text{ m}^2/\text{g}$ , a total pore volume of  $0.09417 \text{ cm}^3/\text{g}$ , and an average pore size of  $25.96 \text{ nm}$ . The catalyst exhibited type IV isotherms with an H1 hysteresis loop, as shown in Figure 5, implying a narrow range of uniform mesopores [33].

Figure 6 shows the TEM images of the carbon support and NiMo/C catalyst that were used for exploring catalyst morphologies. The image showed dark spots, which is an indication of the successful impregnation of the metals onto the support material and their dispersal across ed on the support. The catalyst had an average particle size of approximately  $9.73 \pm 0.46 \text{ nm}$ , as shown in Figure 7.

### 3.3 Optimization of dodecane production

As reported in the previous section, the highest

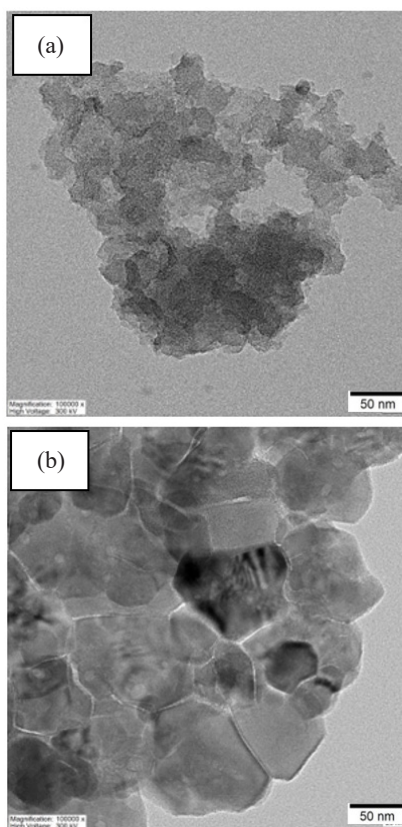


**Figure 6:** TEM images of carbon support (a) and NiMo/C catalyst (b).

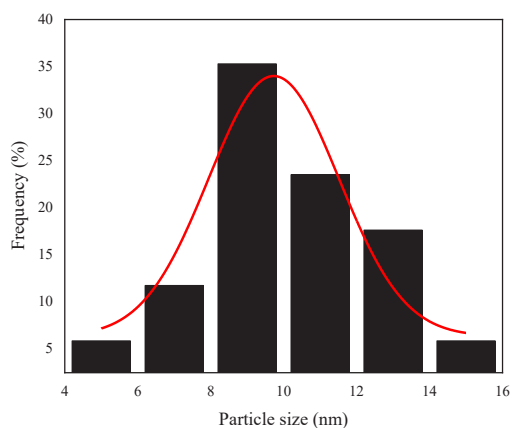


**Figure 7:** particle size distribution of NiMo/C catalyst.

dodecane yield was achieved using the NiMo/C catalyst. The optimization of the operating conditions for dodecane production was studied based on applying the CCD approach.

**Table 3:** Experimental responses based on CCD for dodecane production

Run	Independent Variables		Response Factor
	Temperature (°C)	Pressure (bar)	Dodecane Yield (%)
1	320	22	58.61
2	280	28	33.01
3	300	21	61.53
4	320	28	65.66
5	300	29	55.44
6	300	25	61.51
7	328	25	62.55
8	300	25	44.98
9	280	22	56.89
10	272	25	25.70

Table 3 summarizes ten experiments of the CCD and the results for dodecane yield. The liquid product from the hydrodeoxygenation reaction of methyl laurate was found only as undecane and dodecane. The optimum operating conditions, using a temperature of 320 °C and pressure of 28 bar, produced methyl laurate conversion of 98.26% and had the highest dodecane selectivity of 66.82% and yield of 65.66%.

RSM was used to assess the effects of the three independent parameters and their interactions on the response factor (dodecane yield). The coefficient of determination for the model had a favorable value of  $R^2 = 0.7576$ , indicating a good fit between the model and the observed data.

The normal probability plot of the residuals, shown in Figure 8, revealed a linear trend in the behavior of the residuals, thereby corroborating the assumption that the error terms followed a normal distribution.

The predicted second-order polynomial model in terms of actual factors was:

$$Yield (\%) = 95.7856 + 7.38365A - 99.9876B + 0.128875AB - 0.016775A^2 + 1.25639 B^2 \quad (8)$$

where  $A$  is the temperature (°C) and  $B$  is the pressure (bar).

3D surface plot graphic representations of Equation (8) were used to investigate factor effects. Figure 9 illustrates the effect of temperature and pressure on the dodecane yield. At pressures lower than 25 bar, the temperature had the least effect on the dodecane yield compared to the other factors, with a

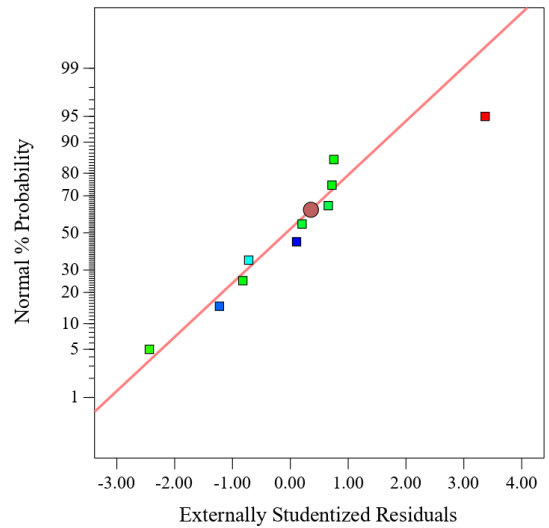


**Figure 8:** Normal plot of residuals.

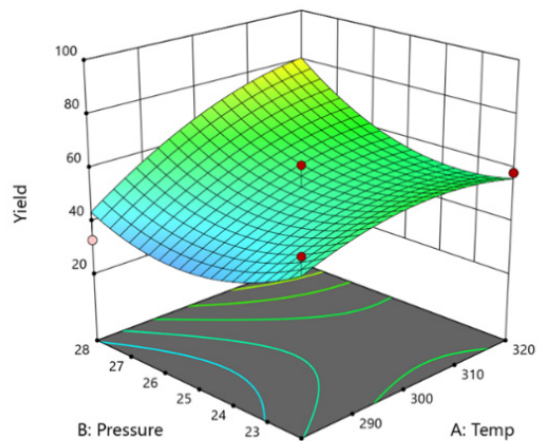


**Figure 9:** Response surface 3D plots showing the effect of temperature and pressure of dodecane yield.

slight increase from 50 to 56 wt.%. On the other hand, the temperature had a greater effect when using high pressure (>25 bar). At higher pressure, the dodecane yield had a sharp increase from 44 to 80%. The results were similar to other previous deoxygenation studies that temperature and pressure were important to the dodecane yield [31], [32].

#### 4 Conclusions

This study investigated the deoxygenation reaction using methyl laurate over Ni/Al<sub>2</sub>O<sub>3</sub>, Ni/C, NiMo/

$\text{Al}_2\text{O}_3$ , NiMo/C, and NiMo/SiO<sub>2</sub>TiO<sub>2</sub> catalysts under conditions of 300 °C and 25 bar for 6 h. The NiMo/C catalyst used for converting methyl laurate to dodecane for use as the solvent in bio-hydrogenated diesel produced the highest conversion and yield of 62.46% and 40.36%, respectively, due to the synergistic effect between the Ni and Mo metals. The optimum operating conditions were determined based on CCD as 320°C and 28 bar, which produced a conversion of 98.26%, dodecane selectivity of 66.82%, and a yield of 65.66%. The response surface data showed temperature had a greater effect when applied using high pressure.

### Acknowledgments

The authors acknowledge the Office of National Higher Education Science Research and Innovation Policy Council - PMU C, PTT EXPLORATION AND PRODUCTION PUBLIC Co.,Ltd., CHERDCHAI CORPORATION Co.,Ltd., POLAWAT ENGINE Co.,Ltd., VERASUWAN Co.,Ltd., (C04F660060). This research was funded by Kasetsart University through the Graduate School Fellowship Program and was supported by the Faculty of Engineering, Kasetsart University and the Kasetsart University Research Development Institute (KURDI).

### Author Contributions

O.P.: Methodology, Validation, Formal analysis, Investigation, Writing - Original Draft; C.P.: Conceptualization, Funding acquisition, Validation, Writing - Review & Editing, Supervision; S.T.: Methodology, Investigation; J.L.: Methodology, Investigation; S.D.: Validation, Writing - Review & Editing, Supervision; S.A. Writing - Review & Editing, Supervision; P.P.: Conceptualization, Resources, Validation, Writing - Review & Editing, Visualization, Supervision, Project administration. All authors have read and agreed to the published version of the manuscript.

### Conflicts of Interest

The authors declare no conflict of interest.

### References

- [1] L. C. Meher, D. V. Sagar, and S. N. Naik, "Technical aspects of biodiesel production by transesterification—a review," *Renewable and Sustainable Energy Reviews*, vol. 10, no. 3, pp. 248-268, 2006, doi: 10.1016/j.rser.2004.09.002.
- [2] R. Heede, "Tracing anthropogenic carbon dioxide and methane emissions to fossil fuel and cement producers, 1854–2010," *Climatic Change*, vol. 122, no. 1, pp. 229–241, 2014, doi: 10.1007/s10584-013-0986-y.
- [3] S. Kawichai, S. Sillapapiromsuk, and S. Bootdee, "Health risk assessment of gaseous pollutants in the ambient environment of Rayong City, Thailand: The initiative of the EEC area," *Applied Science and Engineering Progress*, vol. 16, no. 4, 2023, Art. no. 6755, doi: 10.14416/j.asep.2023.02.009.
- [4] Y.-S. Cheng, P. Mutrakulcharoen, S. Chueter, K. Cheenkachorn, P. Tantayotai, E. J. Panakkal, and M. Sriariyanun, "Recent situation and progress in biorefining process of lignocellulosic biomass: Toward green economy," *Applied Science and Engineering Progress*, vol. 13, no. 4, pp. 299–311, 2020, doi: 10.14416/j.asep.2020.08.002.
- [5] V. G. Yadav, G. D. Yadav, and S. C. Patankar, "The production of fuels and chemicals in the new world: Critical analysis of the choice between crude oil and biomass vis-à-vis sustainability and the environment," *Clean Technologies and Environmental Policy*, vol. 22, no. 9, pp. 1757–1774, 2020, doi: 10.1007/s10098-020-01945-5.
- [6] J. Chen, H. Shi, L. Li, and K. Li, "Deoxygenation of methyl laurate as a model compound to hydrocarbons on transition metal phosphide catalysts," *Applied Catalysis B: Environmental*, vol. 144, pp. 870–884, 2014, doi: 10.1016/j.apcatb.2013.08.026.
- [7] P. Mäki-Arvela, M. Snåre, K. Eränen, J. Myllyoja, and D. Y. Murzin, "Continuous decarboxylation of lauric acid over Pd/C catalyst," *Fuel*, vol. 87, no. 17, pp. 3543–3549, 2008, doi: 10.1016/j.fuel.2008.07.004.
- [8] L. Yang and M. A. Carreon, "Deoxygenation of palmitic and lauric acids over Pt/ZIF-67 membrane/zeolite 5A bead catalysts," *ACS*

- Applied Materials & Interfaces*, vol. 9, no. 37, pp. 31993–32000, 2017, doi: 10.1021/acsami.7b11638.
- [9] M. Snåre, I. Kubičková, P. Mäki-Arvela, K. Eränen, and D. Murzin, “Heterogeneous catalytic deoxygenation of stearic acid for production of biodiesel,” *Industrial & Engineering Chemistry Research*, vol. 45, 2006, doi: 10.1021/ie060334i.
- [10] R. Loe, K. Huff, M. Walli, T. Morgan, D. Qian, R. Pace, Y. Song, M. Isaacs, E. Santillan-Jimenez, and M. Crocker, “Effect of Pt promotion on the Ni-Catalyzed deoxygenation of tristearin to fuel-like hydrocarbons,” *Catalysts*, vol. 9, no. 2, 2019, doi: 10.3390/catal9020200.
- [11] C.-W. Lee, P.-Y. Lin, B.-H. Chen, R. G. Kukushkin, and V. A. Yakovlev, “Hydrodeoxygenation of palmitic acid over zeolite-supported nickel catalysts,” *Catalysis Today*, vol. 379, pp. 124–131, 2021, doi: 10.1016/j.cattod.2020.05.013.
- [12] N. Hongloi, P. Prapainainar, and C. Prapainainar, “Review of green diesel production from fatty acid deoxygenation over Ni-based catalysts,” *Molecular Catalysis*, vol. 523, 2022, Art. no. 111696, doi: 10.1016/j.mcat.2021.111696.
- [13] G. Li, L. Chen, R. Fan, D. Liu, S. Chen, X. Li, and K.H. Chung, “Catalytic deoxygenation of C18 fatty acid over supported metal Ni catalysts promoted by the basic sites of ZnAl<sub>2</sub>O<sub>4</sub> spinel phase,” *Catalysis Science & Technology*, vol. 9, no. 1, pp. 213–222, 2019, doi: 10.1039/C8CY02027B.
- [14] A. N. Kay Lup, F. Abnisa, W. M. A. W. Daud, and M. K. Aroua, “A review on reaction mechanisms of metal-catalyzed deoxygenation process in bio-oil model compounds,” *Applied Catalysis A: General*, vol. 541, pp. 87–106, 2017, doi: 10.1016/j.apcata.2017.05.002.
- [15] K.-W. Jeon, J.-O. Shim, J.-W. Cho, W.-J. Jang, H.-S. Na, H.-M. Kim, Y.-L. Lee, B.-H. Jeon, J.W. Bae, and H.-S. Roh, “Synthesis and characterization of Pt-, Pd-, and Ru-promoted Ni–Ce<sub>0.6</sub>Zr<sub>0.4</sub>O<sub>2</sub> catalysts for efficient biodiesel production by deoxygenation of oleic acid,” *Fuel*, vol. 236, pp. 928–933, 2019, doi: 10.1016/j.fuel.2018.09.078.
- [16] K. Kon, W. Onodera, S. Takakusagi, and K.-i. Shimizu, “Hydrodeoxygenation of fatty acids and triglycerides by Pt-loaded Nb<sub>2</sub>O<sub>5</sub> catalysts,” *Catalysis Science & Technology*, vol. 4, no. 10, pp. 3705–3712, 2014, doi: 10.1039/C4CY00757C.
- [17] S. Chen, G. Zhou, H. Xie, Z. Jiao, and X. Zhang, “Hydrodeoxygenation of methyl laurate over the sulfur-free Ni/γ-Al<sub>2</sub>O<sub>3</sub> catalysts,” *Applied Catalysis A: General*, vol. 569, pp. 35–44, 2019, doi: 10.1016/j.apcata.2018.10.014.
- [18] L. Fu, W. Ba, Y. Li, X. Li, J. Zhao, S. Zhang, and Y. Liu, “Hydrodeoxygenation of non-edible bio-lipids to renewable hydrocarbons over mesoporous SiO<sub>2</sub>-TiO<sub>2</sub> supported NiMo bimetallic catalyst,” *Applied Catalysis A: General*, vol. 633, 2022, Art. no. 118475, doi: 10.1016/j.apcata.2021.118475.
- [19] H. Imai, M. Abe, K. Terasaka, T. Suzuki, X. Li, and T. Yokoi, “Hydroconversion of methyl laurate over silica-supported Ni–Mo catalysts with different Ni sizes,” *Fuel Processing Technology*, vol. 180, pp. 166–172, 2018, doi: 10.1016/j.fuproc.2018.08.014.
- [20] M. Ameen, M. T. Azizan, S. Yusup, A. Ramli, M. Shahbaz, and A. Aqsha, “Process optimization of green diesel selectivity and understanding of reaction intermediates,” *Renewable Energy*, vol. 149, pp. 1092–1106, 2020, doi: 10.1016/j.renene.2019.10.108.
- [21] M. Mahfud and A. Ansori, “Box-behnken design for optimization on biodiesel production from palm oil and methyl acetate using ultrasound assisted interesterification method,” *Periodica Polytechnica Chemical Engineering*, vol. 66, 2021, doi: 10.3311/PPCh.17610.
- [22] S. N. Zdainal Abidin, H. V. Lee, J. C. Juan, N. A. Rahman, and Y. H. Taufiq-Yap, “Production of green biofuel by using a goat manure supported Ni–Al hydrotalcite catalysed deoxygenation process,” *RSC Advances*, vol. 9, no. 3, pp. 1642–1652, 2019, doi: 10.1039/C8RA07818A.
- [23] R. Chajjalearn, K. Padernchok, S. Korkerd, B. Thumthanaruk, V. Rungardthong, W. Visessanguan, D. Uttapap, and B. Lamsal, “Optimization of extrusion process for pentosanase-supplemented swine feed: Evaluation of physical properties and enzyme stability,” *Applied Science and Engineering Progress*, vol. 16, no. 1, 2022, Art. no. 5859, doi: 10.14416/j.asep.2022.04.001.

- [24] N. Junnienkul, M. Sriariyanun, T. Douzou, S. Asavasanti, and P. Yasurin, "Optimization of alkyl imidazolium chloride pretreatment on rice straw biomass conversion," *KMUTNB: International Journal of Applied Science and Technology*, vol. 11, no. 3, pp. 199–207, 2018, doi: 10.14416/j.ijast.2018.06.002.
- [25] B. Sankha, "Central composite design for response surface methodology and its application in pharmacy," in *Response Surface Methodology in Engineering Science*, K. Palanikumar, Ed. Rijeka: IntechOpen, 2021, p. 1–19.
- [26] B. H. Susanto, M. B. Prakasa, and M. H. Shahab, "Synthesis of renewable diesel through hydrodeoxygenation reaction from nyamplung oil (*Calophyllum Inophyllum* oil) using NiMo/Z and NiMo/C catalysts with rapid heating and cooling method," in *IOP Conference Series: Materials Science and Engineering*, 2016, vol. 162, no. 1, Art. no. 012009.
- [27] Z. Hajamini, M. A. Sobati, S. Shahhosseini, and B. Ghobadian, "Waste fish oil (WFO) esterification catalyzed by sulfonated activated carbon under ultrasound irradiation," *Applied Thermal Engineering*, vol. 94, pp. 141–150, 2016.
- [28] N. Chen, S. Gong, and E. W. Qian, "Effect of reduction temperature of NiMoO<sub>3</sub>-x/SAPO-11 on its catalytic activity in hydrodeoxygenation of methyl laurate," *Applied Catalysis B: Environmental*, vol. 174–175, pp. 253–263, 2015, doi: 10.1016/j.applthermaleng.2015.10.101.
- [29] A. Amin, "Review of diesel production from renewable resources: Catalysis, process kinetics and technologies," *Ain Shams Engineering Journal*, vol. 10, no. 4, pp. 821–839, 2019, doi: 10.1016/j.asej.2019.08.001.
- [30] X.-Y. Liu, M. Huang, H.-L. Ma, Z. Zhang, J.-M. Gao, Y.-L. Zhu, X.-j. Han, and X. Guo, "Preparation of a carbon-based solid acid catalyst by sulfonating activated carbon in a chemical reduction process," *Molecules (Basel, Switzerland)*, vol. 15, pp. 7188–7196, 2010, doi: 10.3390/molecules15107188.
- [31] H. O. Hassani and F. Wadaani, "Preparation, characterization and catalytic activity of Nickel Molybdate (NiMoO<sub>4</sub>) nanoparticles," *Molecules*, vol. 23, p. 273, 2018, doi: 10.3390/molecules23020273.
- [32] R.-H. Zhang, Z.-H. Hao, L.-Y. Shi, H.-T. Chen, Y.-C. Shu, and J.-L. He, "Mechanism of non-contact reduction of MoO<sub>3</sub> to prepare MoO<sub>2</sub>," *JOM*, vol. 74, no. 7, pp. 2742–2749, 2022, doi: 10.1007/s11837-022-05282-4.
- [33] M. Thommes, K. Kaneko, A. Neimark, J. Olivier, F. Rodriguez-Reinoso, J. Rouquerol, and K. Sing, "Physisorption of gases, with special reference to the evaluation of surface area and pore size distribution (IUPAC Technical Report)," *Pure and Applied Chemistry*, vol. 87, 2015, doi: 10.1515/pac-2014-1117.